Towards a Quantitative Cartography of the Grain Boundary Energy Landscape: Paths and Correlations

Sterling G. Baird[a,*], Eric R. Homer[a], David T. Fullwood[a], Oliver K. Johnson[a]

[a]*Department of Mechanical Engineering, Brigham Young University, Provo, UT 84602, USA*

Abstract

We apply the Voronoi fundamental zone (VFZ) framework towards gaining insights about the nature of a five degree-of-freedom (5DOF) fundamental zone (FZ) for cubic O_h grain boundaries (GBs). We determine the dimensions of a large O_h VFZ point set, for which the maximum dimension is $\sim$65° after applying a singular value decomposition (SVD) transformation. We also find that nearest neighbor (NN) distances for cubochorically sampled GBs are normally distributed. $\sim$99.6 % of the variance is explained by the first 5 transformed coordinates of the O_h Voronoi fundamental zone grain boundary octonions (VFZ-GBOs), indicating that despite being originally defined by 8D Cartesian coordinates, 5D Cartesian coordinates may be sufficient to describe GBs w.r.t. crystallographic distances. This is in contrast to the classical definition of 5DOF coordinates via inharmonious combination of two very different mathematical objects: a rotation (misorientation) and a vector (plane normal). The 5th transformed dimension is $\sim$70 % the size of the 1st dimension, giving a rough indication of the shape of a 5DOF FZ (i.e. low-aspect ratio). We identify repeated GBs in a large Fe simulation dataset which in turn enables us to estimate the intrinsic uncertainty in the context of experimental measurements and metastable GB states. Gaussian process regression (GPR) allows us to estimate the correlation lengths of the Ni and Fe datasets to be $\sim$7.4° and 8.3°, respectively, compared with a traditionally accepted value of $\sim$10°. That is, the energy of both FCC and BCC GBs are typically correlated within $\sim$11 % to 18 % of the dimensions of the 5DOF FZ. We analyze structure-property paths between the Σ3 coherent-twin (CT) GB and other low-Sigma GBs of interest. The 5DOF path between the FCC-Ni CT Σ3 cusp and a Σ7 cusp are connected (i.e. a direct path exists without an energy barrier), suggesting that the Σ7 cusp will spontaneously transform into the global minimum CT Σ3 cusp (i.e. the transformation is thermodynamically favorable w.r.t. energy minimization). Future work involves probing other cubic and non-cubic symmetries, alloys, and properties such as mobility.

Keywords: Grain Boundary, Structure-Property Model, Interpolation, Octonion, Machine Learning

1. Introduction

When subjected to plastic deformation and/or elevated temperatures, the crystallographic character of grain boundaries (GBs) in polycrystalline microstructures can change to reduce the total system energy [REF]. These energy minimizing transformations of GB crystallography constitute trajectories or paths along the GB energy landscape, which is a function over the 5-dimensional (5D) GB character space. Consequently, to understand, model, and predict such transformations and their effects on microstructure evolution, it is necessary to understand these paths and the relationships between GBs that are near each other in that space.

Examples of such spontaneous energy minimiz-

*Corresponding author.

Email address: ster.g.baird@gmail.com (Sterling G. Baird)

ing changes to GB character include the rotation of the GB plane to achieve equilibrium at triple junctions [REF]—both those formed by the intersection of three GBs within a polycrystal and those formed between a GB and two free surfaces at the exterior of a microstructure. It is this phenomenon that is exploited to produce the quarter- and half-loop bicrystal geometries used in classic constant-driving-force GB migration experiments [REF]. The inclination of the GB plane can also change during GB migration [REF], or upon the disappearance of a grain during grain growth, which requires establishment of new equilibrium configurations at the newly formed triple junctions. This class of energy minimizing changes to GB character constitute paths through the GB energy landscape that are restricted to two-dimensional sub-manifolds (the GB plane fundamental zone (FZ) for a fixed misorientation).

Another class of energy minimizing changes to GB character are illustrated by the phenomenon of grain rotation [REF], which can occur during high-temperature plastic deformation [REF] or recrystallization [REF], as well as at lower temperatures in nanocrystalline materials [REF]. The primary feature of grain rotation is the change in crystal orientation of one grain relative to its neighbors resulting in lower-energy GBs between them. However, when the misorientation between two grains changes there will also be an accompanying change to the GB plane inclination[1]. Consequently, such GB character transformations represent more general paths through the 5D GB character space that are not restricted to any misorientation or boundary plane subspaces.

Until recently, models for GB energy that depend on their full 5D crystallographic character were unavailable. The first such model was developed by Bulatov, Reed, and Kumar (BRK) [1] by fitting a closed-form function to GB energies from a database [2] of 388 GBs in several materials. This function has been employed in a variety of applications to study mesoscale microstructure phenomena like X [REF], Y [REF], and Z [REF]. We recently developed a general approach, called the Voronoi fundamental zone (VFZ) framework, for inferring GB structure-property models from GB structure-property databases [REF].

In this work we present 5D GB structure-property models for FCC Ni and BCC Fe developed using the VFZ framework. We also study correlations in GB energy as a function of crystallographic distance. We use the VFZ framework to give context to GB property correlation lengths and shows that previous estimates are likely too high. We investigate general paths through the GB energy landscape and show qualitatively distinct types of relationships between important types of GBs.

2. Methods

We provide brief summaries of methods related to VFZ construction (Section 2.1.1), interpolation (Section 2.2), path visualization (Section 2.5), and the literature datasets used (Section 2.6).

2.1. The Voronoi Fundamental Zone Framework

We describe the definition of a VFZ (Section 2.1.1), mapping grain boundary octonions (GBOs) into the VFZ (Section 2.1.2), distance calculations (Section 2.1.3), and provide a brief comparison with the traditional GBO metric (Section 2.1.4). The methods are based on functions and scripts from (`github.com/sgbaird-5dof/interp`).

2.1.1. Defining the Voronoi Fundamental Zone

To define a VFZ, an arbitrary, fixed, low-symmetry reference GBO is chosen (o_{ref}) and for our use of GBOs, the VFZ is defined as the region of $\mathbb{S}^7$ (the unit 7-sphere in 8 dimensions) closer to o_{ref} than any of its symmetric images. If a low-symmetry GB is chosen, the point within a VFZ will be unique within numerical tolerance (and hence it is a true FZ). Additionally, we use a Euclidean approximation to the true geodesic distance.

[1]Even if the GB plane remains fixed in the macroscopic reference frame, a change in the GB misorientation results in a change of the GB normal in the crystal reference frame, which is the physically relevant reference frame.

2.1.2. Mapping GBs to the Voronoi Fundamental Zone

A GBO is mapped into a VFZ by calculating the pairwise distances between the reference GBO and each of the symmetrically equivalent octonions[2] and taking the symmetrically equivalent octonion closest to the reference GBO.

2.1.3. Distance Calculations in the Voronoi Fundamental Zone

Once a GBO has been mapped into a VFZ, distance calculations proceed without further consideration of symmetrically equivalent octonions. The VFZ framework suffers from occasional, large distance overestimation which imposes a local sparseness of data and lead to poorer interpolation near the borders of a VFZ. However, this can be mitigated through ensemble or data augmentation techniques.

2.1.4. Comparison with Traditional GBO Framework

The primary differences between the VFZ framework and traditional GBO distance metric are that the VFZ framework is defined by a continuous set of points, exhibits occasional distance overestimation, uses a Euclidean approximation, and has a lower computational complexity.

2.2. Interpolation in the Voronoi Fundamental Zone Framework

While four interpolation methods were tested in the VFZ framework, we focus on GPR which in our case imposes the assumption that crystallographically similar GBs share similar grain boundary energys (GBEs) within some correlation length. GPR has the added benefit of built-in uncertainty quantification.

2.3. Dimensionality Reduction

A SVD transformation is used to remove degenerate dimensions and rotate/align the VFZ-GBO point clouds such that the 1st, 2nd, 3rd, etc. dimensions are progressively smaller.

Additionally, principal component analysis is applied and the variance explained by each dimension is extracted.

2.4. Correlation Matrices

A squared exponential kernel is used as the covariance function:

$$k(x_i, x_j|\theta) = e^{-\frac{1}{2}\frac{\left(x_i - x_j\right)^{\mathsf{T}}\left(x_i - x_j\right)}{{\sigma_l}^2}} {\sigma_f}^2 \qquad (1)$$

where σ_f, σ_l, θ, x, and $\cdot^{\mathsf{T}}$ represent signal standard deviation, length scale (i.e. correlation length), unconstrained positive-bounding parameterization of σ_f and σ_l, VFZ coordinates, and transpose operator, respectively. Conversion to correlation matrices and processing of the data [JOHNSON].

2.5. Visualizing 5DOF Paths

Direct paths between two GBs in a VFZ are obtained via coordinate interpolation constrained to a hyperspherical arc. The direct path in a VFZ is not always the minimum distance path (which may cross the borders of a VFZ). However, it is instructive to observe these paths because the minimum distance path in 5DOF space is not necessarily the path a GB will take during grain growth.

A "tunnel"[3] plot is formed by calculating up to the 6th NNs of the input data relative to the direct path formed between two GBs. The distances of the NNs relative to the arc are used to both color and size the markers on the plot; NN which are closer to the arc are large, blue circles, whereas NN which are further from arc are small, red circles. Additionally, the 1st NN path is plotted as a dashed line.

2.6. Literature Datasets

Ni [5] and Fe [6] GBE datasets from the literature are used. Intrinsic uncertainty for the Fe simulation data is estimated by the following steps:

[2] Contrary to Francis et al. [3] which uses the passive convention for misorientation, we employ the active convention [4].

[3] Similar to traveling through a 1D tunnel but also looking at nearby points in the region close to the line in all directions.

1. Sort GBs into degenerate sets
2. Determine the average GBE for each degenerate set
3. Compare each of the degenerate GBs to the set-wise average GBE (root mean square error (RMSE) or mean absolute error (MAE))

See Section S1 for further details on methods used to estimate intrinsic uncertainty of the Fe simulation dataset.

3. Results

We use the VFZ framework to explore properties of a 5DOF FZ. We address the following questions:

- What is the intrinsic uncertainty of non-globally-optimized molecular statics (MS) simulations relative to the global minimum GBE? (Section 3.4)
- When working with randomly generated, symmetrized VFZ-GBO, how does the number of GBs affect the density and distribution of points? (Section 3.1)
- What are the dimensions of a 5DOF fundamental zone? (Section 3.2)
- How correlated are nearby GBs w.r.t. crystallography and GBE? (Section 3.3)
- What can crystallographic paths in 5DOF space teach us about material behavior? (Section 3.5)

3.1. Density and Distribution of Points

Figure 2 illustrates how the VFZ-GBO average NN distance varies with the cardinality of the set (i.e. number of random VFZ-GBOs in the set). The average NN distance (over approximately 70 trials) of set sizes between 388 and 50 000 between $(10.7175 \pm 0.3684)^\circ$ and $(2.6479 \pm 0.2254)^\circ$, respectively. Additionally, a line fit is given. For a specific 50 000 VFZ-GBO set, the NN GBO distance is $(2.870\,90 \pm 0.691\,12)^\circ$ (Figure 1a) while the average 100-th NN distance is within 10° (Figure 1b).

This indicates that, on average, prediction VFZ-GBOs fall within a typically reported GB correlation length[4] of 10° [7] or 15° [5]) of input VFZ-GBOs in large set sizes. We demonstrate that these correlation lengths may be somewhat overestimated (Section 3.3).

3.2. Dimensions of a VFZ

The maximum dimension of a particular SVD transformed O_h cubic VFZ is ∼65°. The sizes for this first and the remaining 7 dimensions are given in Table 1.

Table 1: Dimension of SVD transformed coordinates (Dimension) and GBO dimension size (ω) for a set of 50 000 VFZ-GBOs. These are the diagonal entries of the "S" matrix in the SVD decomposition.

Dimension	ω (°)
1	65.03
2	63.24
3	58.8
4	53.7
5	46.34
6	6.651
7	5.821
8	2.436e-13

We also find that the largest minimum (i.e. symmetrized) distance (with a VFZ ensemble set size of 20 [4]) between any two GBs in a set of 20 000 GBs is ∼64.0°.

By performing principal component analysis, we find that ∼99.6 % of the variance is explained by the first 5 transformed coordinates of an O_h VFZ as shown in Table 2.

3.3. Correlation Lengths

We present global (Section 3.3.1) and pairwise (Section 3.3.2) correlations for the Ni and Fe simulation datasets.

[4] Correlation length in the context of GBs has been described as "the degree to which boundaries with the same macroscopic geometrical degrees of freedom in different materials have related properties" [5]

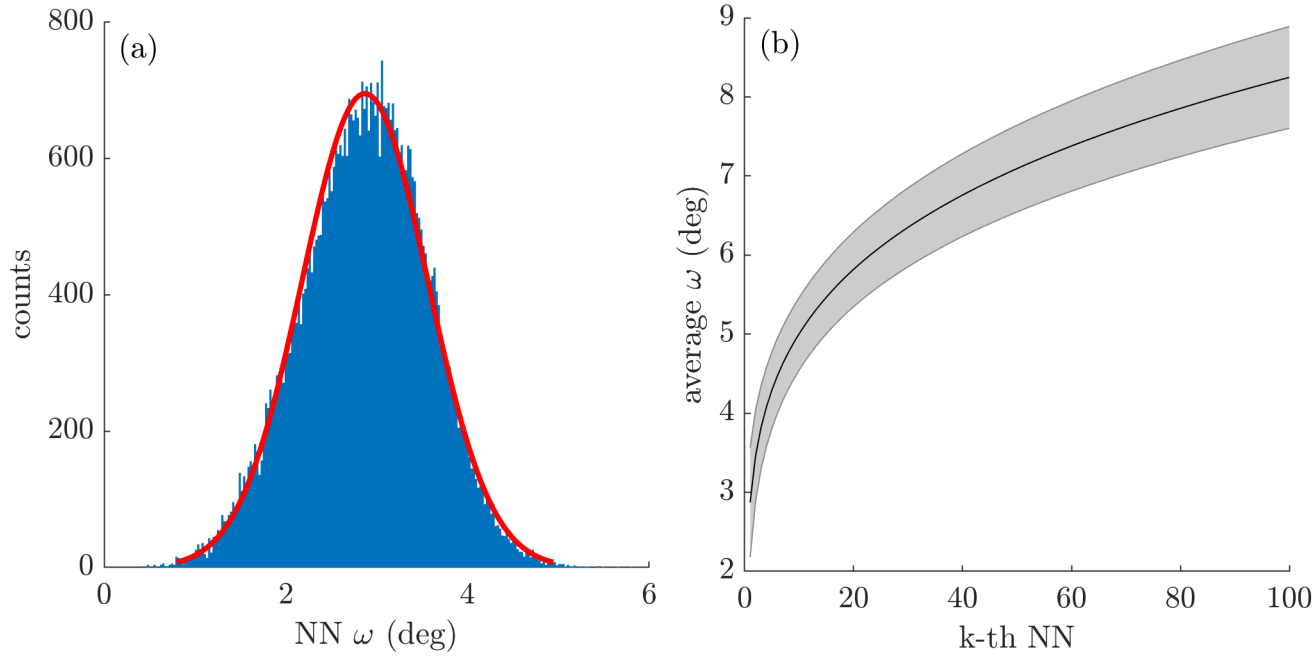

Figure 1: (a) Histogram of NN GBO distances (ω) in a VFZ-GBO set of 50 000 points. The average NN distance was $(2.870\,90 \pm 0.691\,12)^\circ$. (b) The average k-th nearest neighbor distances demonstrate that many nearest neighbors fall within a tight tolerance (less then 10°) out of approximately 10 trial runs.

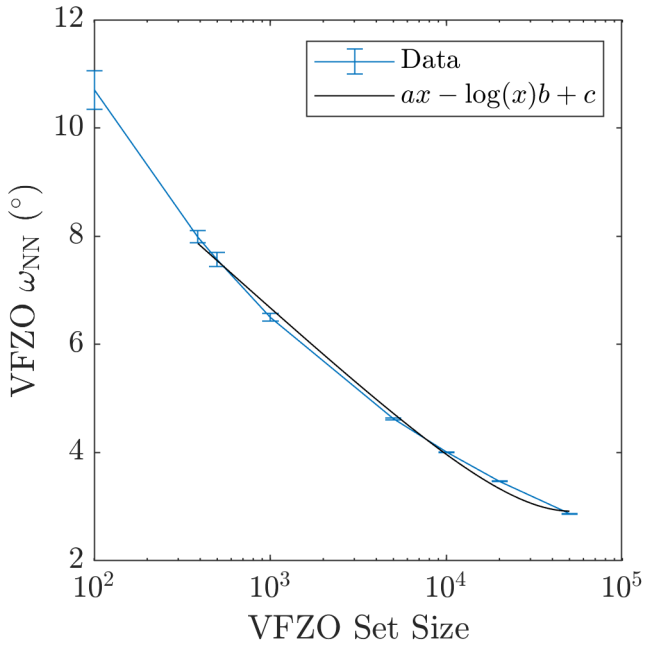

Figure 2: NN VFZ-GBO (ω_{NN}) distances (°) versus VFZ-GBO set size out of 70-80 random VFZ-GBO sets per set size and a fit to $ax - \log(x)b + c$ where $a = 2.5025 \times 10^{-5}$, $b = 1.27396$, $c = 15.4499$, x represents set size, and $388 \leq x \leq 50000$.

Table 2: Dimension of principal component analysis transformed coordinates (Dimension) and percent variance explained (ρ) for a set of 50 000 VFZ-GBOs. The first 5 dimensions cumulatively explain ∼99.6 % of the variance.

Dimension	ρ (%)
1	25.19
2	23.82
3	20.6
4	17.18
5	12.79
6	0.2631
7	0.1565
8	3.532e-28

3.3.1. Global Correlation Lengths

GPR facilitates analytically solving for correlation lengths, which are determined to be ∼7.4° and 8.3° for the Ni and Fe datasets, respectively. If low noise is assumed for Ni, the correlation length drops to ∼2 degrees. See Table 3 for GPR parameters for each dataset.

By contrast, if a GPR model is trained on a large set of 50 000 GBs sampled from the Bulatov

Table 3: Fitted parameters for two GPR models fitted to the 388 simulated Ni GBEs by Olmsted et al. [2] and fitted parameters for a GPR model trained on 80% of the Fe simulation data (46 883 GBs). The first Ni model allows σ to vary, whereas the second constrains σ to be fixed. Mat., σ_L, σ_F, β, and σ are the material (i.e. element), kernel length scale (°), signal standard deviation (Jm^{-2}), constant basis function (Jm^{-2}), and input property standard deviation (Jm^{-2}), respectively.

Mat.	Fix σ	σ_L (°)	σ_F	β	σ
Ni	no	7.3995	0.2049	1.0913	0.0321
Ni	yes	1.9354	0.201	1.1044	0.0001
Fe	no	8.3073	0.0716	1.2192	0.0562

Reed Kumar (BRK) model, the analytic correlation length is 10.5°.

3.3.2. Pairwise Correlations

3.4. Intrinsic Uncertainty of Noisy Molecular Statics Simulations

We estimate the intrinsic uncertainty of an Fe 0 K MS simulation dataset to be 0.065 29 J m^{-2} and 0.061 90 J m^{-2} depending on whether RMSE or MAE estimates are used, respectively. Minimum and maximum error was -0.2625 J m^{-2} and 0.2625 J m^{-2}, respectively.

3.5. 5DOF Paths and GB Behavior

We analyze direct connections between low Sigma GBs of interest to the materials science community. Using the set of 388 GBs defined by Olmsted et al. [5], we choose the Σ5, Σ7, Σ9, and Σ11 GBs with the lowest GBE out of the Olmsted et al. [5] Ni dataset[5]; we then visualize direct paths in a VFZ between each of these and the global minimum Σ3 CT GB (Figure 3). This is performed for both the BRK and VFZ-GPR models.

Likewise, we perform GPR for the Fe simulation dataset for GBs of interest and visualize these using tunnel plots (Figure 4).

[5]The IDs that correspond to each of the low-Σ GBs used for path visualization for the Olmsted et al. [5] and Kim et al. [6] datasets are given in Table 1 and Table 2, respectively.

4. Discussion

We discuss VFZ dimensions (Section 4.1), correlation lengths (Section 4.2), crystallographic paths (Section 4.5), the potential to differentiate w.r.t. 5DOF grain boundary character (Section 4.3), and issues related to the literature datasets that were used (Section 4.4).

4.1. Dimensions of a VFZ

What does it mean that the 5th dimension is ∼70 % the size of the 1st dimension? This gives an indication of the shape of the VFZ. The information-dense dimension sizes are approximately isotropic, indicating a space that is not a perfect hypersphere or hypercube, but somewhat hyper-elliptical or hyper-rectangular.

Could correlation lengths be treated separately by rotating a VFZ such that misorientation and boundary plane normals each align with certain dimensions?

4.2. Correlation Lengths

We discuss global (Section 4.2.1) and pairwise (Section 4.2.2) correlations. We also discuss the latter in the context of Brandon's criteria [**?**].

4.2.1. Global Correlation Length

The two simulation datasets have distinct differences from each other, as summarized in Table 4.

Table 4: Comparison of Ni (Olmsted et al. [5]) and Fe (Kim et al. [6]) MS simulation datasets. The differences in noise-levels results from whether multiple initial starting configurations were probed in search of a globally minimized configuration as opposed to using a single metastable configuration.

Property	Ni	Fe
Size	388	58604
Noise	Low	High
Symmetry	FCC	BCC

Despite these differences in terms of noise, dataset size, and crystal symmetry, it is interesting to see that the analytic correlation lengths within

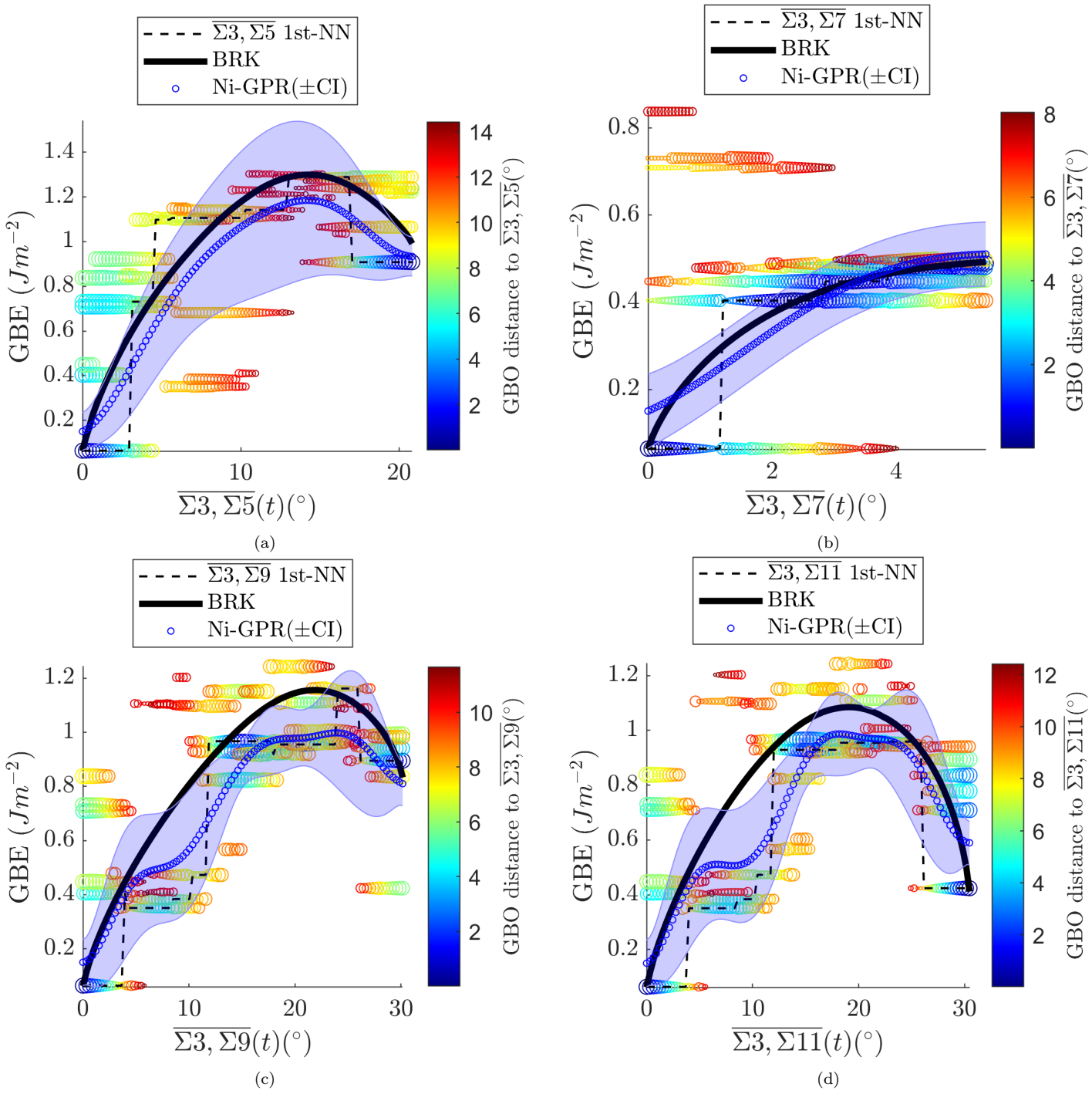

Figure 3: GBEs along direct paths in a VFZ between the Σ3 CT boundary and minimum GBE (a) Σ5, (b) Σ7, (c) Σ9, and (d) Σ11 GBs within the Ni Olmsted et al. [5] dataset. GBE values are plotted for the BRK and GPR models which both used Olmsted et al. [5] as input data. 95% confidence intervals are plotted for the GPR model.

a VFZ are similar for the two datasets. Both are lower than the correlation lengths of 10° [7] and 15° [5] previously reported[6]. It is reasonable to assume that the Ni data has low noise through use

[6]Both of these lengths are based on results from Olmsted et al. [5]

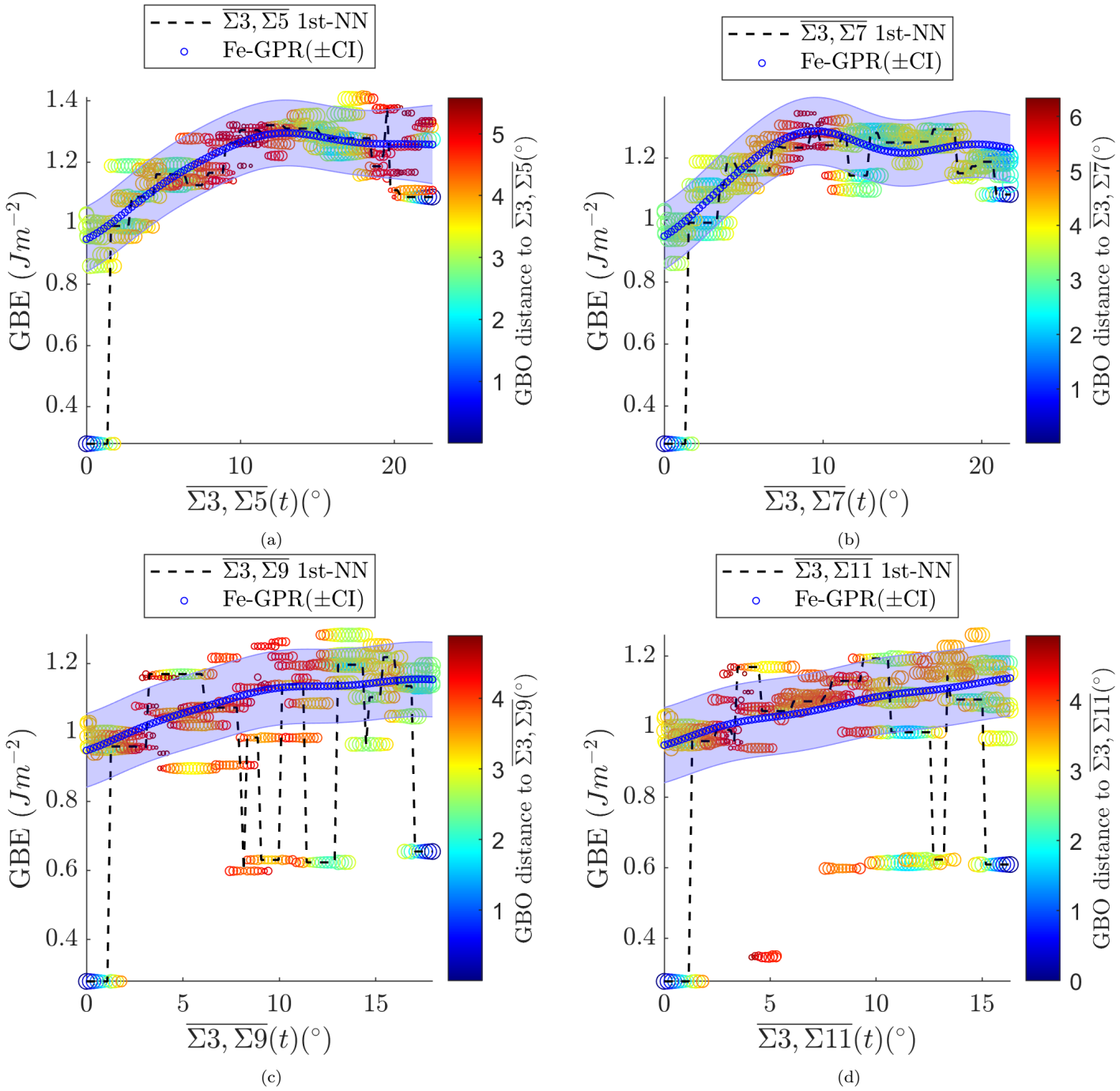

Figure 4: GBEs along direct paths in a VFZ between the minimum GBE Σ3 and minimum GBE (a) Σ5, (b) Σ7, (c) Σ9, and (d) Σ11 GBs for the Fe Kim et al. [6] dataset. A GPR model trained on all 58 604 Fe Kim et al. [6] simulation datapoints was used. 95% confidence intervals are plotted for the GPR model.

of a global optimization strategy[5]; however, the low correlation length of ∼1.9° after imposing the low-noise condition suggests that the Ni dataset may have an actual correlation length much smaller than previously reported. By contrast, the correlation length of a GPR model trained on many BRK GBEs remains relatively large at 10.4°, suggesting that the BRK model is smoothed more than the data warrants on its own. What are the implications? We propose the following:

1. More sophisticated methods are required which do not impose a-priori information

about the correlation length[7], but rather let the data itself suggest proper correlation lengths

2. Larger, low-noise datasets which span all 5DOF are necessary to be confident in structure-property paths that are not restricted to a single misorientation fundamental zone or boundary plane fundamental zone

We believe that the GPR model within the VFZ framework meets the requirements of point #1 and is capable of handling the ideal dataset proposed in point #2.

Some questions that remain are:

- Does the similarity between correlation lengths for FCC and BCC extend to non-cubic crystal symmetries?
- What are the differences in correlation length for other properties? (e.g. mobility)

It is possible that the correlation length will increase with the size of the VFZs, and we expect that the correlation length will depend on the property of interest.

4.2.2. Pairwise Correlations and Brandon's Criteria

[JOHNSON]

4.3. Potential for Numerical Derivatives

GB path visualizations in the VFZ framework suggest the ability to estimate numerical derivatives or gradients of GB properties without being restricted to a GB subspace (e.g. misorientation fundamental zone or boundary plane fundamental zone) which can be a useful mathematical construct for the GB community. For example, steepest descent paths and all local GBE minima can be estimated and used in grain growth simulations.

Because distance overestimation exist in the VFZ framework, use of ensembled VFZ-GBO interpolation or data augmentation may be necessary to mitigate discontinuity artifacts when crossing the exterior of a VFZ as discussed in Section 2.1.3. Alternatively, the "excess" points in a gridded sampling can act as a type of data augmentation and help to address this issue. We plan to explore these topics in future work. Section S2 contains further discussion of a gridded sampling approach.

4.4. Literature Datasets

We analyze implications of results for a Gaussian process regression mixture model developed for a noisy, Fe MS simulation dataset. We find that:

- the model error is on par with the intrinsic uncertainty of the data (Section 4.4.1)
- the predictions likely exhibit overprediction bias relative to the true minimum for a given GB (Section 4.4.2)
- future availability of multiple metastable state GBEs is anticipated to greatly improve the model performance (Section 4.4.3)

We now elaborate each of these points.

4.4.1. Intrinsic Uncertainty

First, because only a single metastable state was used for each GBE simulation, both the training and validation data are subject to noise, consistent with a wide lateral spread of predictions and the intrinsic uncertainty estimation (Figure S2). The Fe simulation dataset Gaussian process regression mixture model gives lower RMSE ($0.055\,035\,\mathrm{J\,m^{-2}}$) and MAE ($0.039\,185\,\mathrm{J\,m^{-2}}$) than the uncertainty estimates. This indicates that the uncertainty itself is somewhat overestimated[8]. The fact that both model and uncertainty metrics are relatively close and the prediction [4] and uncertainty parity plots

[7] The a-priori information that the BRK model imposes is that correlation lengths within a misorientation fundamental zone or boundary plane fundamental zone hold for arbitrary paths through 5DOF space and that moving from one subspace to another results in monotonic behavior.

[8] The prediction error of a model typically cannot be less than the noise of the prediction data of a model even if the model is estimating the true prediction values with better accuracy than the noise (which is very possible and even expected with GPR models when the noise in the input data is approximately Gaussian).

(Figure S2b) are similar suggests that the model is performing well. It also suggests that further improvements in the model relative to the "true" values will be "hidden", i.e. they will probably not manifest as lower RMSE or MAE nor as more tightly distributed parity plots, etc.

4.4.2. Overprediction Bias

Next, given the theoretical existence of a true minimum GBE for a given GB, the predictions which were based on metastable GBEs can be assumed to have an overprediction bias relative to the true minimum. On average, we expect this overprediction bias relative to the true minimum GBE (rather than the most likely metastable state) may be on the order of a few hundred $\mathrm{mJ\,m^{-2}}$ and may vary as a function of true minimum GBE. In other words, the model obtained is probably an estimate of the most likely metastable GBE rather than the true minimum GBE. This is akin to saying that we obtain from this data a model that approximates the non-equilibrium, Stillinger quenched red curve of Figure 4(c1) in [8], not the minimum GBE blue curve of the same chart. See [8] for an in-depth treatment of equilibrium and metastable GBE.

4.4.3. Improving on Existing Datasets

Finally, datasets where multiple metastable GBEs (e.g. 3-10 repeats) are provided for each GB will likely greatly improve the performance of the GPR model in predicting either the most likely metastable GBE (when all GBEs are considered) or the true minimum GBE (when only the minimum GBE is considered for each GB) and may even negate the need for a Gaussian process regression mixture approach. Thus, it is suggested that, where feasible, future large-scale GB bicrystal simulation studies report all property data for repeated trial runs rather than a single trial run or a single value from a set of trial runs. Ideally, data for the three additional microscopic degrees of freedom for GBs (which falls into the category of epistemic uncertainty in this work) would also be included. We believe it is likely that minimum energy paths (i.e. paths of steepest descent) in the GBE landscape depend on both macroscopic and microscopic degrees of freedom (in total, 8DOF) and could offer a more holistic view of GB behavior that better mimics and explains experimental grain growth observations. Indeed, it has been experimentally observed that at least some GB migration mechanisms involve structural transformations between equilibrium GBs via metastable states [9].

4.5. 5DOF Paths

For the GPR model trained on the Ni Olmsted et al. [5] dataset, we observe that $\Sigma3$ and $\Sigma7$ are connected (i.e. no activation energy barrier) while the direct paths between $\Sigma3$ and $\Sigma5$, $\Sigma9$, $\Sigma11$ are separated by energy barriers. This indicates that for grain growth systems governed by GBE, $\Sigma7$ GBs will spontaneously transform into $\Sigma3$ CT GBs, whereas if $\Sigma5$, $\Sigma9$, $\Sigma11$ transform into $\Sigma3$ CTs, this will need to occur either by overcoming the activation energy or via paths through 5DOF space other than the ones shown.

For the GPR model trained on the Fe Kim et al. [6] dataset, the 1st NN path and the GPR path have substantial deviation from each other for the paths from $\Sigma3$ to $\Sigma9$ and $\Sigma3$ to $\Sigma11$. While the GPR model suggests that $\Sigma3$ and $\Sigma11$ are connected, the NN path suggests that there are local minima that are overestimated due to the large noise associated with the Fe dataset.

5. Conclusion

We applied the VFZ framework to learning more about the nature of a 5DOF FZ. The increase of distance computation throughput and the development of a 5DOF VFZ with continuous coordinates enabled us to explore the nature of a 5DOF FZ. We found that symmetrized NN distances are Gaussian and plotted these as a function of set size. We determined the maximum dimension of a particular O_h VFZ to be $\sim65^\circ$.

Other point groups (in particular those which are noncentrosymmetric) may give rise to differently shaped/larger VFZs and for which the Euclidean approximation may need to be removed. It will be interesting to see the VFZ framework applied for other distance metrics (see Morawiec [10] for a comprehensive summary of metrics). The interpolation errors for a Fe simulation dataset are on par

with the intrinsic uncertainty of the dataset itself (Section S1). Analysis of the GPR fitting results indicates that the Ni and Fe simulation datasets have correlation lengths of 8.3° and 7.4°, respectively, but that when the Ni dataset is constrained to have low noise, the analytical correlation length drops to ∼1.9°. Plotting of direct paths between low-Sigma GBs of interest reveal that a Σ7 cusp has a monotonically decreasing path towards the CT Σ3 cusp, whereas a Σ5, Σ9, and Σ11 cusps do not necessarily share this same type of monotonically decreasing path within a VFZ. We demonstrated that two cusps can be connected in 5DOF space.

In addition to its previous implementation for GB property interpolation [4], we anticipate the VFZ framework will continue to reveal important aspects of a 5DOF FZ and inform us about material behavior especially w.r.t. grain growth and other large scale time-dependent or iterative processes.

Acknowledgement

The authors thank Ian Chesser, Toby Francis, Victoria Baird, Brandon Snow, and José Niño for useful discussions. This work was supported by the National Science Foundation under Grant No. 1610077. This work was supported in part through computational resources provided by Brigham Young University's Office of Research Computing.

CRediT Statement

Sterling Baird: Conceptualization, Methodology, Software, Validation, Formal analysis, Investigation, Data Curation, Writing - Original Draft, Writing - Review & Editing, Visualization. **Oliver Johnson**: Supervision, Project administration, Funding acquisition, Conceptualization, Writing - Review & Editing. **David Fullwood**: Funding acquisition, Writing - Review & Editing. **Eric Homer**: Funding acquisition, Writing - Review & Editing

Glossary

5DOF five degree-of-freedom 1, 3, 4, 6, 9–11

BRK Bulatov Reed Kumar 5–9

CT coherent-twin 1, 6, 7, 10, 11

FZ fundamental zone 1, 2, 4, 10, 11

GB grain boundary 1–11

GBE grain boundary energy 3, 4, 6–10

GBO grain boundary octonion 2–5

GPR Gaussian process regression 1, 3, 5–11

MAE mean absolute error 4, 6, 9, 10

MS molecular statics 4, 6, 9

NN nearest neighbor 1, 3–5, 10

RMSE root mean square error 4, 6, 9, 10

SVD singular value decomposition 1, 3, 4

VFZ Voronoi fundamental zone 1–4, 6–11

VFZ-GBO Voronoi fundamental zone grain boundary octonion 1, 3–5, 9

References

[1] V. V. Bulatov, B. W. Reed, M. Kumar, Grain boundary energy function for fcc metals, Acta Materialia 65 (2014) 161–175. doi:10.1016/j.actamat.2013.10.057.

[2] D. L. Olmsted, S. M. Foiles, E. A. Holm, Survey of computed grain boundary properties in face-centered cubic metals: I. Grain boundary energy, Acta Materialia 57 (2009) 3694–3703. doi:10.1016/j.actamat.2009.04.007.

[3] T. Francis, I. Chesser, S. Singh, E. A. Holm, M. De Graef, A geodesic octonion metric for grain boundaries, Acta Materialia 166 (2019) 135–147. doi:10.1016/j.actamat.2018.12.034.

[4] S. G. Baird, E. R. Homer, D. T. Fullwood, O. K. Johnson, Five Degree-of-Freedom Property Interpolation of Arbitrary Grain Boundaries via Voronoi fundamental zone Framework, Computational Materials Science (Under Review) 26.

[5] D. L. Olmsted, E. A. Holm, S. M. Foiles, Survey of computed grain boundary properties in face-centered cubic metals-II: Grain boundary mobility, Acta Materialia 57 (2009) 3704–3713. doi:10.1016/j.actamat.2009.04.015.

[6] H.-K. Kim, S. G. Kim, W. Dong, I. Steinbach, B.-J. Lee, Phase-field modeling for 3D grain growth based on a grain boundary energy database, Modelling and Simulation in Materials Science and Engineering 22 (2014) 034004. doi:10.1088/0965-0393/22/3/034004.

[7] G. S. Rohrer, E. A. Holm, A. D. Rollett, S. M. Foiles, J. Li, D. L. Olmsted, Comparing calculated and measured grain boundary energies in nickel, Acta Materialia 58 (2010) 5063–5069. doi:10.1016/j.actamat.2010.05.042.

[8] J. Han, V. Vitek, D. J. Srolovitz, Grain-boundary metastability and its statistical properties, Acta Materialia 104 (2016) 259–273. doi:10.1016/j.actamat.2015.11.035.

[9] J. Wei, B. Feng, R. Ishikawa, T. Yokoi, K. Matsunaga, N. Shibata, Y. Ikuhara, Direct imaging of atomistic grain boundary migration, Nature Materials (2021). doi:10.1038/s41563-020-00879-z.

[10] A. Morawiec, On distances between grain interfaces in macroscopic parameter space, Acta Materialia 181 (2019) 399–407. doi:10.1016/j.actamat.2019.09.032.